Green Chemistry

ROYAL SOCIETY OF CHEMISTRY

COMMUNICATION

View Article Online
View Journal

Check for updates

Cite this: DOI: 10.1039/d0gc03364b

Received 6th October 2020,
Accepted 16th November 2020

DOI: 10.1039/d0gc03364b

rsc.li/greenchem

Discovering positively charged Pt for enhanced hydrogenolysis of glycerol to 1,3-propanediol†

Binbin Zhao,[a] Yu Liang,[a] Lei Liu, *[a] Qian He *[b] and Jinxiang Dong [a,c]

Atomically-dispersed Pt supported on WO_x-modified tantalum oxide was developed as a highly active catalyst for selective hydrogenolysis of glycerol, with the productivity of 30.80 g g_{Pt}^{-1} h^{-1} toward 1,3-propanediol. The WO_x species pre-deposited on *T*-Ta_2O_5 were found to assist the atomic dispersion of platinum. The WO_x-stabilized $Pt^{\delta+}$ species adsorb hydrogen easily and facilitate the hydrogen heterolytic dissociation, which significantly enhances the capability of *in situ* generated Brønsted acid sites and the hydrogenation activity. This provides a new strategy for developing bi-functional catalysts for a broad range of hydrogen and acid-involved reaction.

The boom in the biodiesel industry brings about a significant amount of surplus glycerol, thus converting glycerol into value-added chemicals is of great importance to the sustainability of global biodiesel production.[1] Converting glycerol to 1,3-propanediol (1,3-PDO), an important monomer for producing polytrimethylene terephthalate, is an attractive approach that could reduce our dependence on fossil feedstock.[2,3]

Among many recent works on searching for suitable catalysts,[4–13] supported Pt and WO_x catalysts show high commercialization potential due to their superior catalytic performance and high stability. Normally, high loadings of tungsten (*e.g.* 10 wt%) and platinum (*e.g.* 2 wt%) are required to achieve the desired productivity of 1,3-PDO (15.2 g g_{Pt}^{-1} h^{-1}, Table S1†). The active sites are thought to be the interface between the Pt and WO_x species, which are optimized to a certain extent by increasing their loadings.[11,14,15] However, such high loading of Pt and W often results in inactive highly polymerized WO_x species or large particles, leading to a low atomic utilization efficiency and unsatisfying catalytic results.[8,11,16–18] Therefore, improving the platinum and WO_x dispersion and further optimize their interaction promises further enhancements for the overall catalytic performance.

It is now widely accepted that glycerol hydrogenolysis to 1,3-PDO over bi-functional catalysts proceeds through dehydration of glycerol to 3-hydroxypropanal (3-HPA) over Brønsted acidic sites followed by consecutive hydrogenation over Pt metal nanoparticles.[19–26] The intermediate of 3-HPA is very unstable and fast hydrogenation of 3-HPA is very crucial to achieve a high selectivity toward 1,3-PDO.[27]

Recently, atomically dispersed platinum catalysts as hydrogenation active sites were widely studied, showing high activity and selectivity for the hydrogenation of substrates containing polar functional groups.[28–30] For example, Yan *et al.* reported a stable Pt single-atom catalyst using phosphomolybdic acid-modified active carbon as support, in which the positively charged Pt could adsorb hydrogen easily, showing a high hydrogenation activity in the case of the substrate containing –C=O group.[29] Inspired by this, we prepared a positively charged single/pseudo-single atom Pt catalyst on WO_x-modified tantalum oxide, achieving high productivity of 1,3-PDO (30.80 g g_{Pt}^{-1} h^{-1}) for glycerol hydrogenolysis. Such high catalytic performance was attributed to both the high dispersion of Pt and an optimized interface between Pt and WO_x species. The crystalline T-phase Ta_2O_5 (*T*-Ta_2O_5) was prepared from hydrated oxide ($Ta_2O_5 \cdot nH_2O$) by calcination at 900 °C,[31] and was chosen as support owing to its outstanding thermal and hydrothermal stability, and the high similarity with W-species in electronegativity and ionic radius which would be helpful to enhance the dispersion of WO_x species on its surface.[32] Especially, the negligible acidic property for *T*-Ta_2O_5 could minimize glycerol dehydration on the support, and allow us to investigate the reaction mechanism over the Pt and WO_x-based catalysts. *T*-Ta_2O_5 with nano-scale size (~200 nm) was prepared using a solvothermal method followed by calcination at 900 °C (ESI†). To ensure the high dispersion of WO_x on the *T*-Ta_2O_5 surface, a simple impregnation–centrifugation method has

[a]College of Chemistry and Chemical Engineering, Taiyuan University of Technology, Taiyuan, Shanxi 030024, P. R. China. E-mail: liulei@tyut.edu.cn
[b]Department of Materials Science and Engineering, National University of Singapore, Singapore 117575. E-mail: heqian@nus.edu.sg
[c]School of Chemical Engineering and Light Industry, Guangdong University of Technology, Guangzhou 510006, P. R. China

†Electronic supplementary information (ESI) available. See DOI: 10.1039/d0gc03364b

been developed to load the WO_x species. Platinum was further dispersed onto the $WO_x/T\text{-}Ta_2O_5$ with a second impregnation step (denoted as $Pt^{\delta+}/WO_x/T\text{-}Ta_2O_5$). The essential physicochemical properties of $T\text{-}Ta_2O_5$ before and after loading W and Pt were summarized in Table S2,† wherein the actual loading of W and Pt was determined by ICP-AES method, with 0.68 wt% for Pt and 0.51 wt% for W in a typical $Pt^{\delta+}/WO_x/T\text{-}Ta_2O_5$ catalyst, respectively (Scheme 1).

The structure of $T\text{-}Ta_2O_5$ remains unchanged after loading WO_x and platinum species, as evidenced by powder XRD patterns (Fig. S1†). The absence of Pt and WO_3 nanoparticles diffraction peaks revealed the homogeneous dispersion of Pt metal and low polymerized tungsten oxide species on the support surface.[17,25,33]

Raman and UV-vis characterization was also used to identify the dispersion and the polymerization degree of WO_x species. For $WO_x/T\text{-}Ta_2O_5$ and $Pt^{\delta+}/WO_x/T\text{-}Ta_2O_5$ samples, Raman spectra (Fig. S2†) show there is no typical characteristic peaks for crystalline WO_3 (805 cm^{-1} for W–O stretching, 270 cm^{-1} for W–O–W deformation).[17,18] And only the band at 950–1000 cm^{-1} corresponding to the stretching mode of W═O in the highly dispersed WO_x species was observed.[34–36] The absorption edge of $WO_x/T\text{-}Ta_2O_5$ in UV-vis spectra move to a higher wavelength of 315 nm compared with pristine $T\text{-}Ta_2O_5$ (Fig. S3†), confirming that no high polymerized WO_x species were formed on the $T\text{-}Ta_2O_5$ surface.[37,38] And the band centered around 225nm-260 nm is attributed to isolated tungsten species or low polymeric tungsten oxide species in a distorted tetrahedral or an octahedral coordination environment,[39] the similar results were also observed on the W/SiO_2, and further confirmed by X-ray absorption spectroscopy study.[40] From these results, it can be seen that the developed impregnation–centrifugation method is a powerful strategy to achieve highly-dispersed WO_x species with a low polymeric state on $T\text{-}Ta_2O_5$ surface, which was suggested to be the actual active components combining with Pt species for glycerol hydrogenolysis to 1,3-PDO.[8,11,14]

SEM images show that $Pt^{\delta+}/WO_x/T\text{-}Ta_2O_5$ has a coral-shaped morphology with a particle size of 100–200 nm (Fig. S4†). The dispersion of Pt and WO_x were further investigated using aberration-corrected scanning transmission electron microscopy (STEM). High angle annular dark-field (HAADF) Z-contrast STEM images of the $Pt^{\delta+}/WO_x/T\text{-}Ta_2O_5$ catalyst are shown in Fig. 1(a and b). Ultra-small (*e.g.* 1 nm or less) species can be found on the $T\text{-}Ta_2O_5$ support. The small size and similarity of the atomic number of Ta (Z = 73), W (Z = 74) and Pt (Z = 78) made it difficult to directly differentiate these elements.[9] Therefore, two additional samples were studied for comparison, namely $WO_x/T\text{-}Ta_2O_5$ and $Pt/T\text{-}Ta_2O_5$. WO_x clusters can be found in the $WO_x/T\text{-}Ta_2O_5$ (Fig. 1(c and d)) which are very similar in size compared to the ones in the $Pt^{\delta+}/WO_x/T\text{-}Ta_2O_5$ catalyst. And Pt nanoparticles can be clearly seen from the $Pt/T\text{-}Ta_2O_5$ sample (Fig. 1(e and f)). From these comparisons, it is reasonable to speculate that Pt dispersion has been significantly improved due to the presence of WO_x species deposited priority on the support, acting as anchoring sites. Since no obvious size increase was observed in those clusters shown in Fig. 1(a) compared to Fig. 1(c), it can be inferred that no Pt nanoparticles were formed onto WO_x and Pt is likely to be atomically dispersed on the entire $WO_x/T\text{-}Ta_2O_5$ surface.

Probe molecule infrared (IR) spectroscopy with CO has been widely used to identify the valence state and dispersion for Pt species on the catalyst. Because the adsorbed CO could not be detected on the bare $WO_x/T\text{-}Ta_2O_5$, the peaks upon loading Pt were derived from the CO adsorbed on different Pt species (Fig. 2a). Two dominant peaks at 2138 cm^{-1} and 2091 cm^{-1} for $Pt^{\delta+}/WO_x/T\text{-}Ta_2O_5$ were ascribed to the linearly bonded CO on isolated $Pt^{\delta+}$ species and PtO_x clusters (<1 nm),

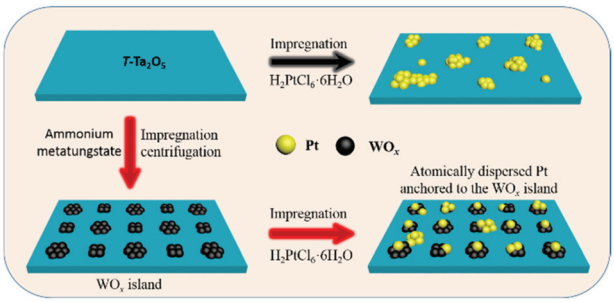

Scheme 1 Illustration of preparation process of $Pt^{\delta+}/WO_x/T\text{-}Ta_2O_5$.

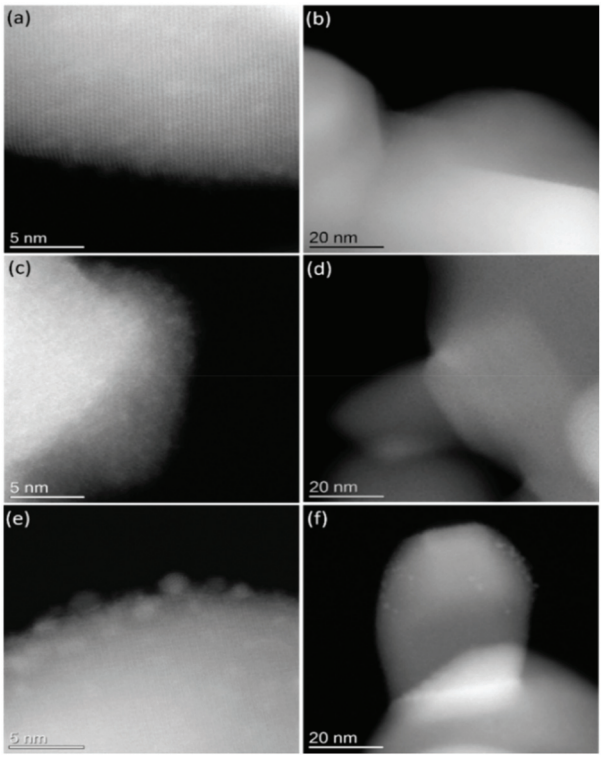

Fig. 1 STEM-HAADF images of (a and b) $Pt^{\delta+}/WO_x/T\text{-}Ta_2O_5$ catalyst, (c and d) $WO_x/T\text{-}Ta_2O_5$ catalyst and (e and f) $Pt/T\text{-}Ta_2O_5$ catalyst.

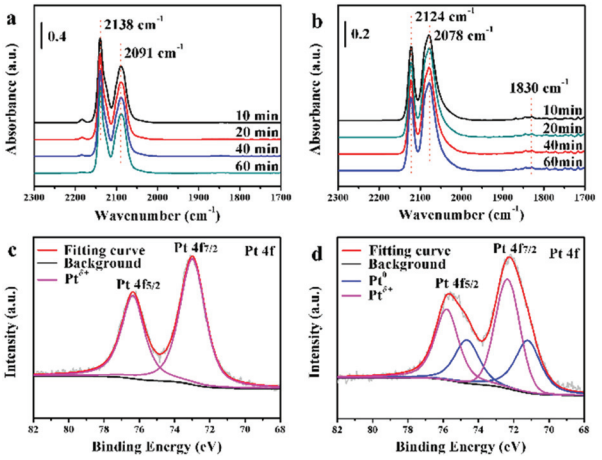

Fig. 2 IR spectra of CO adsorbed on various catalysts during desorption processes, and XPS spectra of Pt 4f: $Pt^{\delta+}/WO_x/T\text{-}Ta_2O_5$ (a and c), $Pt/T\text{-}Ta_2O_5$ (b and d).

respectively.[41–45] For Pt supported catalysts, the peak position for the adsorbed CO molecules are closely associated with the electronic structure of Pt species and the bonding configuration of the Pt to CO.[46,47] The bonding energy of Pt species in $Pt/T\text{-}Ta_2O_5$ is less than that of $Pt^{\delta+}/WO_x/T\text{-}Ta_2O_5$, as confirmed by X-ray photoelectron spectroscopy (Fig. 2), as a result, the peak corresponding to CO adsorbed on isolated $Pt^{\delta+}$ species was red shifted to 2124 cm^{-1} from 2138 cm^{-1} for $Pt/T\text{-}Ta_2O_5$. The peaks at 2078 cm^{-1} and 1830 cm^{-1} are assigned to the linearly bonded CO on Pt nanoparticles and the bridge-bonded CO on Pt nanoparticles in more large size, respectively, while the latter is not observed on $Pt^{\delta+}/WO_x/T\text{-}Ta_2O_5$.[41,42,48] Also, the peak intensity corresponding to the isolated $Pt^{\delta+}$ species in $Pt^{\delta+}/WO_x/T\text{-}Ta_2O_5$ is much higher than that of $Pt/T\text{-}Ta_2O_5$, showing that much more isolated Pt species were formed on $WO_x/T\text{-}Ta_2O_5$. The Pt species could be well held in a highly dispersed state by their strong interaction with WO_x islands formed on the $T\text{-}Ta_2O_5$ surface.

The electronic state of the two supported Pt catalysts were further investigated with X-ray photoelectron spectroscopy (XPS). XPS spectra (Fig. 2c) show that only cationic platinum species between those of Pt(II) and Pt(IV) were detected in $Pt^{\delta+}/WO_x/T\text{-}Ta_2O_5$ catalysts. It should be noted that the Pt 4f bands shift to the higher binding energies (Pt $4f_{5/2}$ 72.98 eV and Pt $4f_{7/2}$ 76.36 eV) after depositing WO_x species on the support, indicating the strong interaction between the Pt and WO_x species behaved on the support surface. According to H_2-TPR test results (Fig. S5†), the main reduction peaks of $Pt^{\delta+}$ species on $Pt^{\delta+}/WO_x/T\text{-}Ta_2O_5$ occurs at 545 °C that is higher than that of WO_x-free catalysts, while the H_2 consumed for reduction of $Pt^{\delta+}$ species is greater than that observed on $Pt^{\delta+}/T\text{-}Ta_2O_5$ with the same Pt content, indicating that the strong metal–support interaction (SMSI) between Pt and $WO_x/T\text{-}Ta_2O_5$ as well as a more high-dispersion of Pt species on $WO_x/T\text{-}Ta_2O_5$. Based on TEM, IR, XPS, and H_2-TPR results, we can conclude that the isolated $Pt^{\delta+}$ species and platinum oxide clusters were highly dispersed on the surface of the support, and the SMSI between Pt and WO_x assure the $Pt^{\delta+}$ species to disperse at the atomic-level.[9,49]

The catalytic properties in the glycerol hydrogenolysis were shown in Table 1. It can be seen that $Pt^{\delta+}/WO_x/T\text{-}Ta_2O_5$ catalyst exhibits significantly high catalytic activity and selectivity toward 1,3-PDO (1,3-PDO/1,2-PDO molar ratio = 68.61) compared to the pristine $T\text{-}Ta_2O_5$ supported Pt catalyst. Moreover, the catalytic results of glycerol hydrogenolysis over $Pt^{\delta+}/WO_x/T\text{-}Ta_2O_5$ (Table S3†) during the reaction process indicated that the selectivity of 1,3-PDO was stable, showing excellent performance for the selective cleavage of the second C–O bond of glycerol. The nature and the number of acidic sites on catalysts are also very important to glycerol hydrogenolysis. The NH_3-TPD and FTIR of adsorbed pyridine over catalysts were performed to reveal the acidic property (Fig. S6 and S7†), however, only the weak Lewis acid sites in Py-IR spectra were observed on $Pt^{\delta+}/WO_x/T\text{-}Ta_2O_5$, which is associated with the presence of terminal W=O group upon loading WO_x species on $T\text{-}Ta_2O_5$. Generally, Brønsted acid sites play a crucial role to achieve a high selectivity toward 1,3-PDO in glycerol hydrogenolysis over bi-functional catalysts.[5,8,17] To confirm if the protonic acid site could be *in situ* generated on $Pt^{\delta+}/WO_x/T\text{-}Ta_2O_5$ catalyst during the glycerol hydrogenolysis, the control Py-IR experiment was conducted by co-feeding H_2 with pyridine. Interestingly, we observed a new peak at 1540 cm^{-1} corresponding to the pyri-

Table 1 Catalytic results of glycerol hydrogenolysis over various catalysts in aqueous media[a]

Entry	Catalyst	Time (h)	Conversion (%)	Selectivity (%)				Selectivity ratio (1,3/1,2)
				1,3-PDO	1,2-PDO	2-PrOH	1-PrOH	
1	$WO_x/T\text{-}Ta_2O_5$	12	—	—	—	—	—	—
2	$Pt/T\text{-}Ta_2O_5$	12	3.77	7.24	21.02	5.83	60.93	0.34
3	$Pt^{\delta+}/WO_x/T\text{-}Ta_2O_5$	12	89.88	44.8	0.65	4.42	42.36	68.61
4	$Pt^0/WO_x/T\text{-}Ta_2O_5$[b]	12	22.71	54.35	3.74	5.18	30.92	14.53
5	$Pt^{\delta+}/WO_x/T\text{-}Ta_2O_5$[b]	12	53.71	49.41	1.60	5.58	35.50	30.88
		24	87.00	45.61	0.76	4.15	38.56	63.96

[a] Reaction conditions: 6.184 g of 3 wt% glycerol solution, 0.2 g of catalyst, 160 °C, 5.0 MPa H_2 pressure, stirring rate of 600 rpm. 1-PrOH, 2-PrOH, and 1,2-PDO refer to 1-propanol, 2-propanol, and 1,2-propanediol, respectively. [b] 30 wt% glycerol solution was applied under identical reaction condition.

dine on Brønsted acid sites (Fig. S8†), indicating that the Brønsted acid sites could be available for the first-step dehydration of glycerol by H_2 dissociation over the interface of Pt and WO_x during the reaction. Hydrogen activation is significantly important for the selective hydrogenolysis of glycerol to 1,3-PDO, which is associated with the *in situ* Brønsted acid generation for dehydration and the activated H-species for hydrogenation.[9,10,12] The activation mode of H_2 on atomically dispersed metal species is closely related to the local coordination environment, the hydrogen heterolytic dissociation is more favored on positively charged single atoms than that on metallic atoms.[30] The positively charged Pt species in $Pt^{\delta+}/WO_x/T\text{-}Ta_2O_5$ enable H_2 to heterolytically dissociate to $H^{\delta+}$ and $H^{\delta-}$ species, and $H^{\delta+}$ species spilled over the surface of support *via* Pt–O–W interfacial, forming O–$H^{\delta+}$ and Pt–$H^{\delta-}$ species.[9,50] A control experiment was conducted on $Pt^0/WO_x/T\text{-}Ta_2O_5$ catalyst obtained from $Pt^{\delta+}/WO_x/T\text{-}Ta_2O_5$ by H_2 reduction treatment, in which the Pt species mainly existed in the form of Pt^0, as evidenced by XPS (Fig. S9†). The catalytic results (Table 1, entry 4) show the glycerol conversion on $Pt^{\delta+}$ catalyst is about 2.5 times higher than that on Pt^0 catalyst, indicating that the high catalytic activity is attributed to the $Pt^{\delta+}$–O–W species.[51]

H_2–O_2 titration experiment was carried out to investigate the hydrogen absorption performance of Pt-based catalysts. The H_2 consumption was not detected on $WO_x/T\text{-}Ta_2O_5$ (Fig. S10†) and consequently, any H_2 uptake is attributed to the presence of Pt species on support. Control experiments demonstrate that $Pt^{\delta+}/WO_x/T\text{-}Ta_2O_5$ exhibits a significantly high H_2 adsorption capacity compared to the two other catalysts with the same Pt loading (Fig. 3). The excellent H_2 absorption capability was attributed to the atomically dispersed platinum species, as well as the maximized interface between Pt and WO_x which facilitates the dissociated H-species spillover and form the Brønsted acid sites on the catalyst,[9] implying that $Pt^{\delta+}/WO_x/T\text{-}Ta_2O_5$ has potential in successive hydration–hydrogenation reaction.

It has been recognized that fast hydrogenation of 3-HPA over Pt is a key step for the formation of 1,3-PDO from glycerol hydrogenolysis.[22,23] Since 3-HPA is not stable and not commercially available, we attempted to use propanal as a model molecular to evaluate the hydrogenation activity of the carbonyl group on various Pt containing catalysts. $Pt^{\delta+}/WO_x/T\text{-}Ta_2O_5$ catalyst exhibited much higher activity than that of the reduced catalyst of $Pt^0/WO_x/T\text{-}Ta_2O_5$ in the hydrogenation of propanal to 1-PrOH (Fig. 3d) at room temperature. Based on this fact, we infer that the positively charged Pt species in atomic-level dispersion are ideal active sites compared with metal Pt for the fast hydrogenation of 3-HPA intermediate to 1,3-PDO, further illustrating the applied potential of the positively charged single metal atoms in hydrogen-involved reaction.[29]

Combining the current characterization and catalytic reaction results, a plausible reaction scheme was proposed for glycerol hydrogenolysis on the studied catalyst (Scheme 2). First, hydrogen was absorbed and heterolytically dissociated to $H^{\delta+}$ and $H^{\delta-}$ species over the positively charged Pt single atoms, and $H^{\delta+}$ species could spillover from Pt atoms to the support *via* Pt–O–W interfacial leading to the generation of W–(OH)–Ta species as Brønsted acid sites.[12,52,53] The primary –OH group of glycerol molecular was inclined to chemisorb on the cationic Pt cluster owing to the high charge density. The *in situ* generations of Brønsted acid sites are favorable for eliminating the secondary –OH group to form a secondary carbenium, then 3-HPA by keto–enol tautomerism. The high activity of $Pt^{\delta+}$ species assured the speedy hydrogenation of 3-HPA to 1,3-PDO.

The reusability and stability of $Pt^{\delta+}/WO_x/T\text{-}Ta_2O_5$ were firstly investigated with four successive runs under the regular reaction condition (Table 1, entry 3). After each reaction run, the catalyst was recovered, washed with distilled water and dried at 110 °C temperature before the next reaction. As shown in

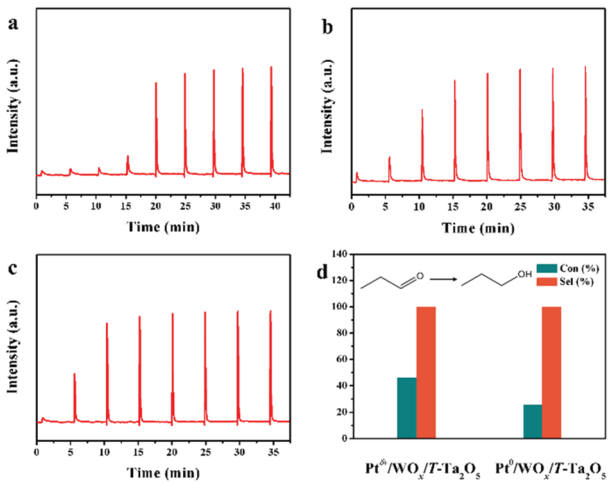

Fig. 3 H_2–O_2 titration profiles $Pt^{\delta+}/WO_x/T\text{-}Ta_2O_5$ (a), $Pt/T\text{-}Ta_2O_5$ (b), $Pt^{\delta+}/WO_x/T\text{-}Ta_2O_5$ (c) and the catalytic results (d) of propanal hydrogenation over various Pt-containing catalysts.

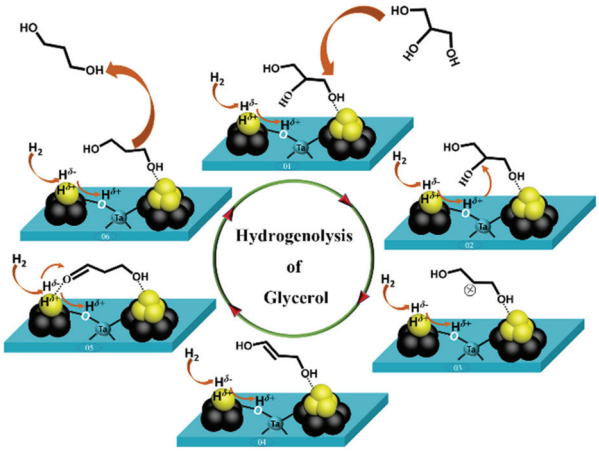

Scheme 2 Proposed reaction mechanism of glycerol hydrogenolysis to 1,3-PDO over $Pt^{\delta+}/WO_x/T\text{-}Ta_2O_5$.

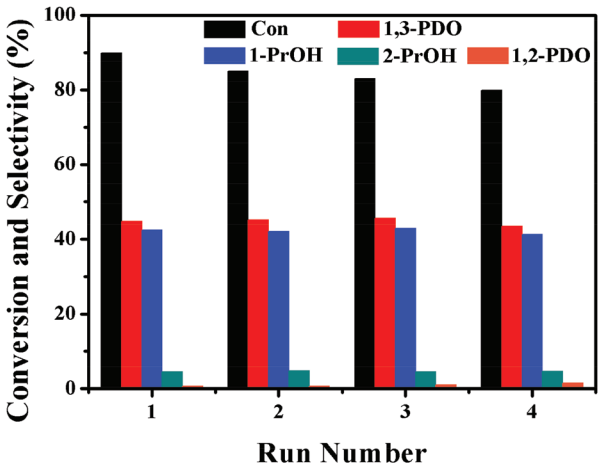

Fig. 4 The conversion and product distribution in glycerol hydrogenolysis over the $Pt^{\delta+}/WO_x/T\text{-}Ta_2O_5$ catalyst in four successive runs.

Fig. 4, the conversion rate of glycerol showed a small decrease from 89.88% to 78.56% after four successive runs, while the selectivity toward 1,3-PDO kept stable at about 45%. It should be noted that, the glycerol conversion dropped relatively quickly (about 6%) after the first run, then very slowly in the next successive runs. Elemental analysis for the reaction liquid was done and no leaching of Pt or W from the catalyst was detected. XPS was used to identify the valence states of Pt-species in the catalyst after the first and 4th run (Fig. S11†), and the fitting results are summarized in Table S4.† It was found that the surface $Pt^{\delta+}/(Pt^{\delta+} + Pt^0)$ ratio in catalyst rapidly decreased to about 55% from 100% after the first run, however, the further reduction of $Pt^{\delta+}$ species had not been obviously observed in the next runs, and there is still more than 44% $Pt^{\delta+}$ species remained on the catalyst even after the 4th run. Therefore, the obvious drop in activity for the 2nd run probably resulted from the reduction of a portion of $Pt^{\delta+}$ species during the reaction, and this easily reducible $Pt^{\delta+}$ species could be ascribed to their weak interaction with WO_x. By contrast, the $Pt^{\delta+}$ species having strong interaction with WO_x could be well kept during reaction owing to its high reduction temperature as confirmed by H_2-TPR results (Fig. S5†), which showed much higher catalytic activity compared to the easily reducible ones. Consequently, the catalytic activity for $Pt^{\delta+}/WO_x/T\text{-}Ta_2O_5$ could remain at a high level in the next successive runs. Moreover, only one peak corresponding PtO_x clusters (<1 nm) was detected in the IR spectra of CO adsorbed on the used catalyst (Fig. S12†), indicating that high dispersed WO_x could enhance the stability of platinum species and effectively inhibit their agglomeration during the reaction. These results certify that $Pt^{\delta+}/WO_x/T\text{-}Ta_2O_5$ catalyst has an operational reusability and remarkable stability in our current reaction condition for the hydrogenolysis of glycerol, and potential in a candidate for practical application.

In conclusion, we prepared a stable positively charged Pt catalyst with atomic-level dispersion by loading an extremely low content of WO_x species on $T\text{-}Ta_2O_5$, exhibiting remarkable productivity of 1,3-PDO in the hydrogenolysis of glycerol, which is much higher than the reported results so far with Pt-WO_x-based catalysts. The superior catalytic performance was attributed to the highly-dispersed $Pt^{\delta+}$ and the strong interaction between Pt and $WO_x/T\text{-}Ta_2O_5$, which facilitates the hydrogen heterolytic dissociation and H-species spillover to produce Brønsted acid sites, and affords a high catalytic activity for hydrogenation. This discovery will be helpful to understand the glycerol hydrogenolysis mechanism, and also provide an ideal in designing powerful bi-functional catalysts for the hydrogen and acid-involved reaction.

Conflicts of interest

There are no conflicts to declare.

Acknowledgements

This work was financially supported by the National Natural Science Foundation (21978194 and U1910202), the Natural Science Foundation of Shanxi Province (Grant No. 201801D121055), and Program for the Shanxi Young Sanjin Scholar. Qian He would like to acknowledge the support by National Research Foundation (NRF) Singapore, under its NRF Fellowship (NRF-NRFF11-2019-0002).

Notes and references

1 M. Pagliaro, R. Ciriminna, H. Kimura, M. Rossi and C. D. Pina, *Angew. Chem., Int. Ed.*, 2007, **46**, 4434–4440.
2 A. M. Ruppert, K. Weinberg and R. Palkovits, *Angew. Chem., Int. Ed.*, 2012, **51**, 2564–2601.
3 U. Witt, R.-J. Müller, J. Augusta, H. Widdecke and W.-D. Deckwer, *Macromol. Chem. Phys.*, 1994, **195**, 793–802.
4 L. Z. Qin, M. J. Song and C. L. Chen, *Green Chem.*, 2010, **12**, 1466–1472.
5 S. Zhu, X. Gao, Y. Zhu, Y. Zhu, X. Xiang, C. Hu and Y. Li, *Appl. Catal., B*, 2013, **140–141**, 60–67.
6 R. Arundhathi, T. Mizugaki, T. Mitsudome, K. Jitsukawa and K. Kaneda, *ChemSusChem*, 2013, **6**, 1345–1347.
7 D. D. Falcone, J. H. Hack, A. Y. Klyushin, A. Knop-Gericke, R. Schlögl and R. J. Davis, *ACS Catal.*, 2015, **5**, 5679–5695.
8 S. García-fernández, I. Gandarias, J. Requies, M. B. Güemez, S. Bennici, A. Auroux and P. L. Arias, *J. Catal.*, 2015, **323**, 65–75.
9 J. Wang, X. Zhao, N. Lei, L. Li, L. Zhang and S. Xu, *ChemSusChem*, 2016, **9**, 784–790.
10 Y. Fan, S. Cheng, H. Wang, D. Ye, S. Xie, Y. Pei, H. Hu, W. Hua, Z. H. Li, M. Qiao and B. Zong, *Green Chem.*, 2017, **19**, 2174–2183.
11 W. Zhou, J. Luo, Y. Wang, J. Liu, Y. Zhao, S. Wang and X. Ma, *Appl. Catal., B*, 2019, **242**, 410–421.
12 T. Aihara, H. Miura and T. Shishido, *Catal. Sci. Technol.*, 2019, **9**, 5359–5367.

13 W. Zhou, Y. Zhao, Y. Wang, S. Wang and X. Ma, *ChemCatChem*, 2016, **8**, 3663–3671.
14 N. Lei, X. Zhao, B. Hou, M. Yang, M. Zhou, F. Liu, A. Wang and T. Zhang, *ChemCatChem*, 2019, **11**, 3903–3912.
15 S. García-Fernández, I. Gandarias, Y. Tejido-Núñez, J. Requies and P. L. Arias, *ChemCatChem*, 2017, **9**, 4508–4519.
16 Y. Fan, S. Cheng, H. Wang, J. Tian, S. Xie, Y. Pei, M. Qiao and B. Zong, *Appl. Catal., B*, 2017, **217**, 331–341.
17 S. Zhu, X. Gao, Y. Zhu and Y. Li, *J. Mol. Catal. A: Chem.*, 2015, **398**, 391–398.
18 S. García-Fernández, I. Gandarias, Y. Tejido-Núñez, J. Requies and P. L. Arias, *ChemCatChem*, 2017, **9**, 4508–4519.
19 J. Chaminand, L. A. Djakovitch, P. Gallezot, P. Marion, C. Pinel and C. Rosier, *Green Chem.*, 2004, **6**, 359–361.
20 T. Miyazawa, Y. Kusunoki, K. Kunimori and K. Tomishige, *J. Catal.*, 2006, **240**, 213–221.
21 E. Tsukuda, S. Sato, R. Takahashi and T. Sodesawa, *Catal. Commun.*, 2007, **8**, 1349–1353.
22 T. Miyazawa, S. Koso, K. Kunimori and K. Tomishige, *Appl. Catal., A*, 2007, **318**, 244–251.
23 I. Gandarias, P. L. Arias, J. Requies, M. B. Güemez and J. L. G. Fierro, *Appl. Catal., B*, 2010, **97**, 248–256.
24 S. Zhu, Y. Qiu, Y. Zhu, S. Hao, H. Zheng and Y. Li, *Catal. Today*, 2013, **212**, 120–126.
25 S. Zhu, X. Gao, Y. Zhu, J. Cui, H. Zheng and Y. Li, *Appl. Catal., B*, 2014, **158–159**, 391–399.
26 D. Coll, F. Delbecq, Y. Aray and P. Sautet, *Phys. Chem. Chem. Phys.*, 2011, **13**, 1448–1456.
27 M. R. Nimlos, S. J. Blanksby, X. Qian, M. E. Himmel and D. K. Johnson, *J. Phys. Chem. A*, 2006, **110**, 6145–6156.
28 H. Wei, X. Liu, A. Wang, L. Zhang, B. Qiao, X. Yang, Y. Huang, S. Miao, J. Liu and T. Zhang, *Nat. Commun.*, 2014, **5**, 1–8.
29 B. Zhang, H. Asakura, J. Zhang, J. Zhang, S. De and N. Yan, *Angew. Chem., Int. Ed.*, 2016, **55**, 8319–8323.
30 Y. Chen, S. Ji, W. Sun, W. Chen, J. Dong, J. Wen, J. Zhang, Z. Li, L. Zheng, C. Chen, Q. Peng, D. Wang and Y. Li, *J. Am. Chem. Soc.*, 2018, **140**, 7407–7410.
31 T. Kitano, S. Okazaki, T. Shishido, K. Teramura and T. Tanaka, *Chem. Lett.*, 2011, **40**, 1332–1334.
32 L. Xu, Y. Wang, X. Yang, X. Yu, Y. Guo and J. H. Clark, *Green Chem.*, 2008, **10**, 746–755.
33 W. Zhang, J. Chen, A. I. Minett, G. F. Swiegers, C. O. Too and G. G. Wallace, *Chem. Commun.*, 2010, **46**, 4824–4826.
34 T. Tsuchiya, H. Imai, S. Miyoshi, P. A. Glans, J. Guo and S. Yamaguchi, *Phys. Chem. Chem. Phys.*, 2011, **13**, 17013–17018.
35 Y. Chen and I. E. Wachs, *J. Catal.*, 2003, **217**, 468–477.
36 U. Balachandran and N. G. Eror, *J. Mater. Sci. Lett.*, 1982, **1**, 219–222.
37 Q. Lin, K. Ichi Shimizu and A. Satsuma, *Appl. Catal., A*, 2009, **365**, 55–61.
38 D. G. Barton, M. Shtein, R. D. Wilson, S. L. Soled and E. Iglesia, *J. Phys. Chem. B*, 1999, **103**, 630–640.
39 S. Maksasithorn, P. Praserthdam, K. Suriye and D. P. Debecker, *Microporous Mesoporous Mater.*, 2015, **213**, 125–133.
40 C. Bisio, A. Gallo, R. Psaro, C. Tiozzo, M. Guidotti and F. Carniato, *Appl. Catal., A*, 2019, **581**, 133–142.
41 M. J. Kale and P. Christopher, *ACS Catal.*, 2016, **6**, 5599–5609.
42 K. Ding, A. Gulec, A. M. Johnson, N. M. Schweitzer, G. D. Stucky, L. D. Marks and P. C. Stair, *Science*, 2015, **350**, 189–192.
43 M. J. Kappers and J. H. van der Maas, *Catal. Lett.*, 1991, **10**, 365–373.
44 E. V. Ramos-Fernández, B. Samaranch, P. R. de la Piscina, N. Homs, J. L. G. Fierro, F. Rodríguez-Reinoso and A. Sepúlveda-Escribano, *Appl. Catal., A*, 2008, **349**, 165–169.
45 O. Pozdnyakova, D. Teschner, A. Wootsch, J. Kröhnert, B. Steinhauer, H. Sauer, L. Toth, F. C. Jentoft, A. Knop-Gericke, Z. Paál and R. Schlögl, *J. Catal.*, 2006, **237**, 1–16.
46 E. Ivanova, M. Mihaylov, F. Thibault-Starzyk, M. Daturi and K. Hadjiivanov, *J. Mol. Catal. A: Chem.*, 2007, **274**, 179–184.
47 G. J. Kim, D. W. Kwon and S. C. Hong, *J. Phys. Chem. C*, 2016, **120**, 17996–18004.
48 B. Qiao, A. Wang, X. Yang, L. F. Allard, Z. Jiang, Y. Cui, J. Liu, J. Li and T. Zhang, *Nat. Chem.*, 2011, **3**, 634–641.
49 O. S. Alexeev, G. W. Graham, M. Shelef and B. C. Gates, *J. Catal*, 2000, **190**, 157–172.
50 L. Bai, X. Wang, Q. Chen, Y. Ye, H. Zheng, J. Guo, Y. Yin and C. Gao, *Angew. Chem., Int. Ed.*, 2016, **55**, 15656–15661.
51 M. N. Taylor, W. Zhou, T. Garcia, B. Solsona, A. F. Carley, C. J. Kiely and S. H. Taylor, *J. Catal.*, 2012, **285**, 103–114.
52 T. Kitano, T. Hayashi, T. Uesaka, T. Shishido, K. Teramura and T. Tanaka, *ChemCatChem*, 2014, **6**, 2011–2020.
53 T. Murayama, N. Kuramata and W. Ueda, *J. Catal.*, 2016, **339**, 143–152.

